ASTFE
American Society
of Thermal and Fluids Engineers

5th Thermal and Fluids Engineering Conference (TFEC)
April 5–8, 2020
New Orleans, LA, USA

TFEC-2019-32417

HYDRAULIC COMPARISON OF SINGLE AND MULTIPLE-JET IMPINGEMENT ON A FLAT PLATE

Ryan S. Reed[1], Abdullah Weiss[1], Paul Kristo[1], Mark L. Kimber[2,*]

[1]Texas A&M University, College Station, TX 77840, USA
[2]Assistant Professor, Department of Nuclear Engineering and Department of Mechanical Engineering
AI Engineering Building 205D, Texas A&M University, College Station, TX 77840

ABSTRACT

Jet impingement onto a solid boundary is of practical interest in a variety of engineering applications. The novelty of the current work is in the comparison of the single and multiple inline jets, the latter being more prevalent in application but less examined in the literature. The study focuses explicitly on the incompressible, hydraulic comparison, by performing experiments near room temperature and low speeds. Three round jets of diameter 22.23 mm are placed inline and 2 diameters apart on the ceiling of the test section. The jets issue vertically downward into a pseudo-unconfined domain whose bottom surface is 9.8 diameters from the jet outlets, acting as the plate. Three distinct flow rates are measured via Stereoscopic Particle Image Velocimetry (S-PIV) for both the single jet and triple jet geometries, where for the latter, each outlet is set to an equivalent flow rate. Several reference parameters further delineate fluid properties in the test section and ambient environment. The investigation begins with evaluation of the single jet, comparing first and second order turbulence statistics with existing literature. The triple jet cases are then presented, showing dramatically different behavior. The results of each configuration, inlet profiles, reference parameters, and uncertainty quantification are provided to embolden future work in computational fluid dynamics (CFD). The investigation concludes with the promotion of several comparisons of the single and triple jet setup and is meant to provide insight into the expected dynamic response of the fluid near and along the solid boundary.

KEY WORDS: Jet impingement; Particle Image Velocimetry; Turbulent mixing

1 INTRODUCTION

The single round jet has received extensive devotion in the literature due to its existence in a variety of real-world applications. The study of such jets exist in fields relative to the design of electronic component cooling [1-4], the mixing of hot and cold fluid streams [5-8], and for this particular study, a preliminary analysis of importance in very high temperature reactors (VHTR).

In the current study, the jet flow conditions are driven by a next generation nuclear reactor design, the prismatic very high temperature reactor (VHTR) [9, 10]. This type of reactor is one of a handful of advanced nuclear reactor designs being considered by the U.S. Department of Energy (DOE). This reactor will implement the cooling medium of the inert helium gas at temperatures up to 850°C. Within the VHTR core, the helium gas flows in the vertical direction downward in circular channels through hexagonal fuel blocks which discharge into the lower plenum. Next the gas is cumulatively routed out of the core through a single outlet. The VHTR goes through a series of complicated flow scenarios. There exists hundreds of coolant channels that combine in the lower plenum, where non-uniform heating in the core yields jets at different temperatures and velocities. The result is temperature fluctuations and gradients that induce thermal stresses on the lower plenum components. The flow is then forced to change direction by 90° traveling through the outlet and toward downstream components for energy generation. Although the flow is extremely complicated,

*Corresponding Author: mark.kimber@tamu.edu

a number of fundamental processes are of utmost importance including turbulent flow past cylinders, jets in cross flow, and even jet impingement.

This study is a part of a superposition validation effort to understand the flow and interactions of this prismatic VHTR. Small scale attempts to validate each simplistic component of this reactor helps understand the complex nature of flow by breaking the large-scale model into multiple small-scale studies. The primary goal of these studies will aid in the development of computational fluid dynamic (CFD) models of each individual study to develop the complex flow physics of the VHTR. This particular study looks at the interaction between the impinging single and triple jets. These jets impinge on a flat plate orthogonal to the downstream flow. Particle image velocimetry measurements are used to obtain flow characteristics such as velocity contours, velocity profiles, and Reynolds stresses. These methods will describe the turbulent behavior of these confined jets and compare the single jet results with the interaction between three jets. Three separate jet velocities are considered at Reynolds numbers of 17121, 20130, and 25682, for case 1, case, 2, and case 3, respectively. The experimental facility and PIV acquisition approach is outlined next, followed by a discussion of results from single and triple jet studies.

2 EXPERIMENTAL METHODOLOGY

The experimental facility is illustrated in Figure 1 and consists of a rectangular test section with an origin at the direct center of the top plate. Depending on the experiment, one or three jets issue into the test section via the top plate. The jet diameter is D = 22.225 mm and is used to non-dimensionalize the spatial coordinates. The test section is $9.79D$ in height and $20.57D$ and $27.43D$ in width and breadth, respectively. Solid walls exist at four of the boundaries while the remaining two ($y = \pm 13.715$ mm) are open to allow outflow. A flow motivation skid is employed to generate the jet flow at prescribed mass flow rates. Upstream conditioning of the jet flow with honeycomb inserts enables a well-characterized velocity profile to be established at the inlet to the test section ($x = 0$). Detailed description of the skid and flow conditioning is provided in [11].

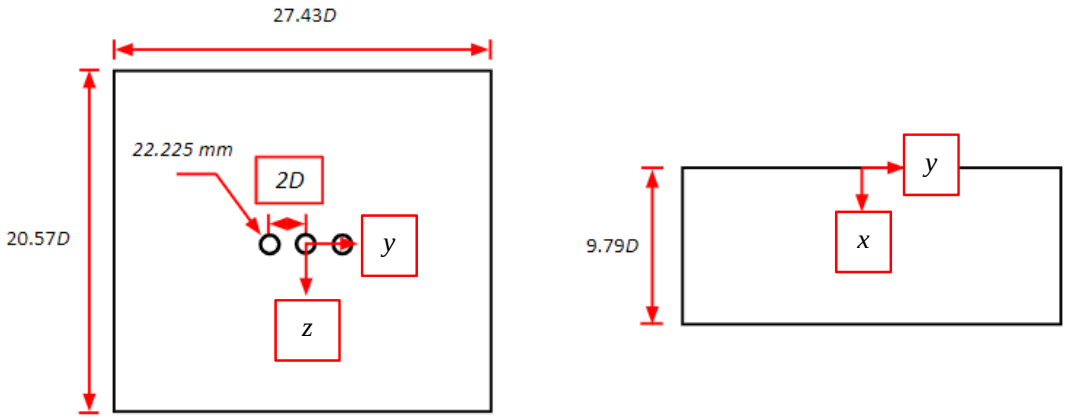

Figure 1: Apparatus setup and reference frame: (a) top view and (b) side view.

The stereo particle image velocimetry (S-PIV) technique is utilized in two principle planes, namely, the centerline xy plane, and the yz-plane at the x/D = 1,2,3,4,6,8 locations. The xy plane measurements serve to analyze the major features of the flow in the streamwise direction while the yz planes provide a qualitative description of the spreading of the jets at cross sections of the principal flow direction. Two high speed Phantom Miro M120 cameras are utilized with 21-bit dynamic range and a resolution of 1920 × 1200 pixels. Camera accessories include a Scheimpflug mount, Nikon AF NIKKOR 50 m f/1.8D lens, and LaVision Inc. 527 nm lens filter with 10 nm band pass and 70% transmission efficiency. A Photonics Industries DM30-527-DH laser with a maximum power of 60 mJ/pulse produces the laser sheet at 527 nm and thickness of approximately 1.0 mm. The flow is seeded with Dioctyl Sebacate using a TSI Six Jet Atomizer Model 9306 upstream of the temperature and flow conditioning to ensure well mixed seeding density at the jet inlets. Three of the atomizer jets are utilized and motivated by an air compressor with a regulated pressure of 413.685 kPa

running for an average of 7 seconds per test. Measurements were captured at 1 kHz for 2.6 seconds for all planes. Typically viewing widow sizes are 159.2 mm × 151.9 mm and 177.2 mm × 151.9 mm for the xy and yz planes, respectively. Typical scaling factors were 5.41209 px/mm and 4.59355 px/mm for the xy and yz planes, respectively.

The high-speed images are then processed using LaVision DaVis 8.4.0 software. The images are pre-processed using a subtract time filter with the average intensity of the entire image ensemble for a given capture, in an effort to reduce undesired ambient noise. Velocity vectors are processed using the stereo cross correlation method. Two initial passes are used with a 64 × 64 pixel interrogation window, 1:1 square grid, and 75% overlap. The remaining four final passes include a 32 × 32 pixel interrogation window, adaptive grid, and 75% overlap. Vector post processing consists of vector removal for values with a peak ratio less than two, followed by a two pass median filter ("strongly remove and iteratively replace" option) for spurious vector removal. The filter removes vectors if their difference from the average is more than two standard deviations than that of its neighbors and subsequently replaces the vector if the difference from average is less than three standard deviations from its neighbors. Finally, ensemble averaged statistics and higher order moments are calculated from the post-processed results.

3 RESULTS

3.1 xy-Plane Velocity Contours

The ensemble-averaged streamwise velocity contours taken in the xy plane in the center of the jet flow are presented in Figure 2 for the single jet and Figure 3 for the triple jet. The velocity profiles are plotted as dimensionless values by dividing by the jets bulk velocity, U_{bulk}. The bulk velocity is the average inlet velocity of the jet, found using a two point calibration of the flow motivation skid [11] and the low and high end of the skid capabilities. Due to the field of view of the Phantom Miro M120, two runs were conducted for a complete case, one run with the camera collecting data from $0D - 4D$ and the second run collecting data from $4D - 8D$. The contours and velocity values are then stitched together to show one complete test section for each case. Since the data is collected using ensemble-averaged values, the data represents statistically steady information which allows the data sets to be combined and considered as one data set. The entrainment of the flow with increasing downstream distances shows that the contour of the flow closely resembles a classical round jet with a peak velocity occurring in the centerline of the jet stream ($y/D = 0$), with an initially sharp velocity gradient, followed by a gradual decrease to zero as y/D increases further in magnitude. The centerline velocity also decays with an increase in the downstream direction (x) as one would expect for a typical jet impingement scenario. The triple jet configuration looks quite similar to three isolated jets when comparing the contours of Figure 2 and Figure 3.

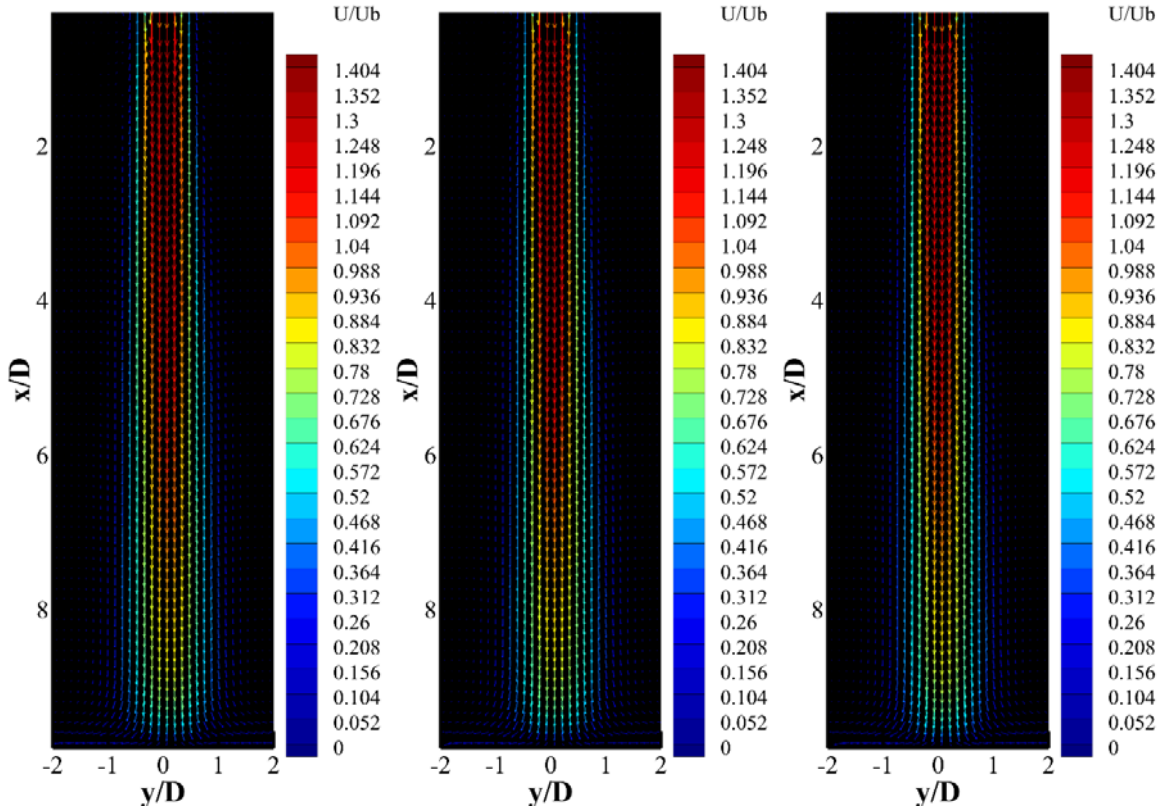

c) Case 1 U_{bulk} = 11.38 m/s b) Case 2 U_{bulk} = 13.27 m/s a) Case 3 U_{bulk} = 17.07 m/s

Figure 2: Velocity contour plots for single jet

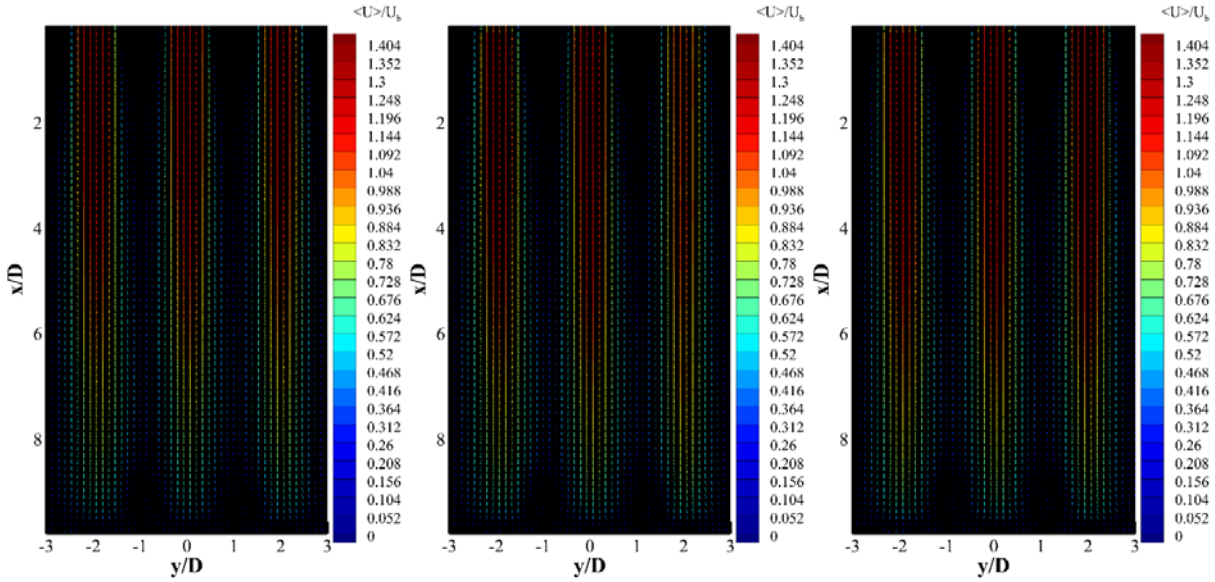

a) Case 1 U_{bulk} = 11.38 m/s b) Case 2 U_{bulk} = 13.27 m/s c) Case 3 U_{bulk} = 17.07 m/s

Figure 3: Velocity contour for triple jet

3.2 Spanwise Velocity Profiles

In order to analyze the data in more detail, traces of the contours from Figure 2 and Figure 3 are provided in Figure 4 and Figure 5 for the single jet and triple jet, respectively. Each figure contains multiple traces across a wide ragne of x/D values for all three cases of jet Reynolds numbers. The velocity profiles are again normalized by the bulk velocity values. In these figures, it become more clear that the $< U >/U_{bulk} > 1$ occurs for the triple jet (Figure 5) while it does not for the single jet (Figure 4). This is likely due to the uncertainty in the two point system calibration. Additional calibration points including repeatability estimations are underway to further minimize this uncertainty, but the current results are still valuable in that they provide insight into the flow physics and relative differences between single and triple jet configurations.

The peak velocity at the jet center (y/D = 0) begins to decay from the inlet value near x/D = 5 for all three single jet cases in Figure 4. This is the location where the potentical core of the jet flow is known to terminate. The maximum velocity then decreases beyond this point and would eventually reach a value of zero at the location of the impingement plate (x/D = 9.8D). Similar trends, namely the existence of the potentical core, are observed for all three cases of triple jet line traces in Figure 5. The jet is also shown to spread in the streamwise direction for both single and triple jet configurations, as one would expect. An interesting feature in Figure 4 (and to a lesser extent in Figure 5) is the region of negative velocities for the profile at x/D = 1. This occurs just beyond the edge of the jet ($y/D \approx \pm 0.7$), and is expected for a non-free jet flow configuration. As the fluid enters the domain via the jet inlet, it is abruptly introduced to a shear layer, and a recirculation region is produced. It is evident that this recirculation region is contained close to the top wall since the location $y/D = \pm 0.7$ has only positive values even at x/D = 2. Similar trends have been noted in other jet impingement applications [4].

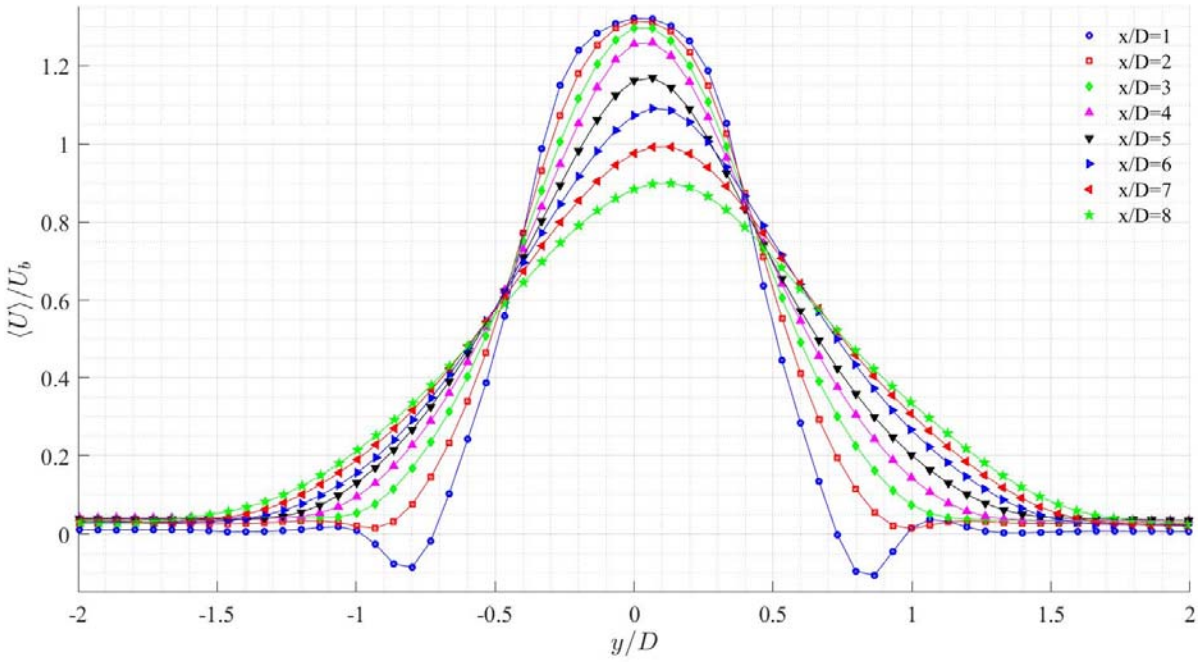

a) Case 1 U_{bulk} = 11.38 m/s

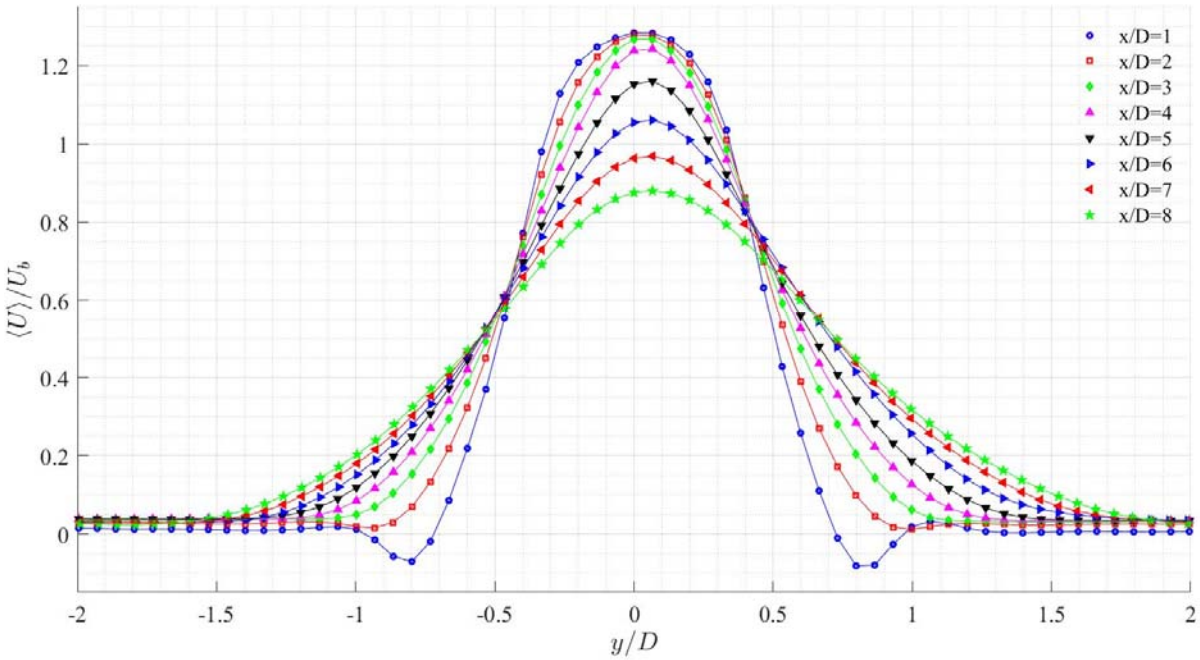

b) Case 2 U_{bulk} = 13.27 m/s

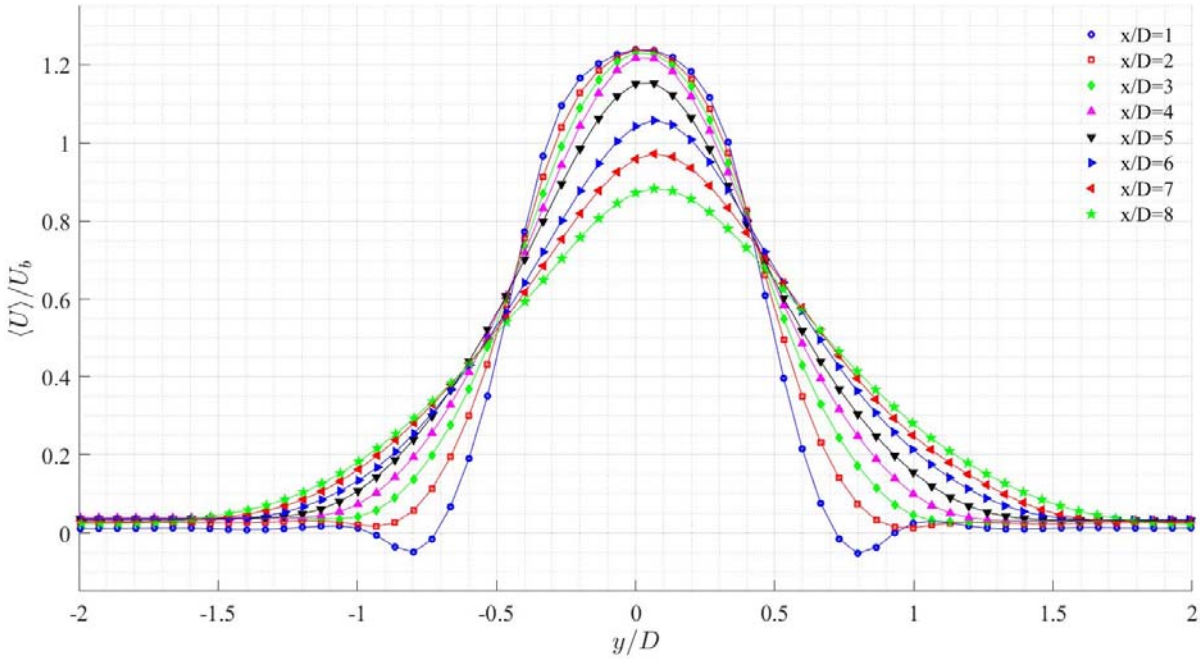

c) Case 3 U_{bulk} = 17.07 m/s

Figure 4: Velocity profile for single jet

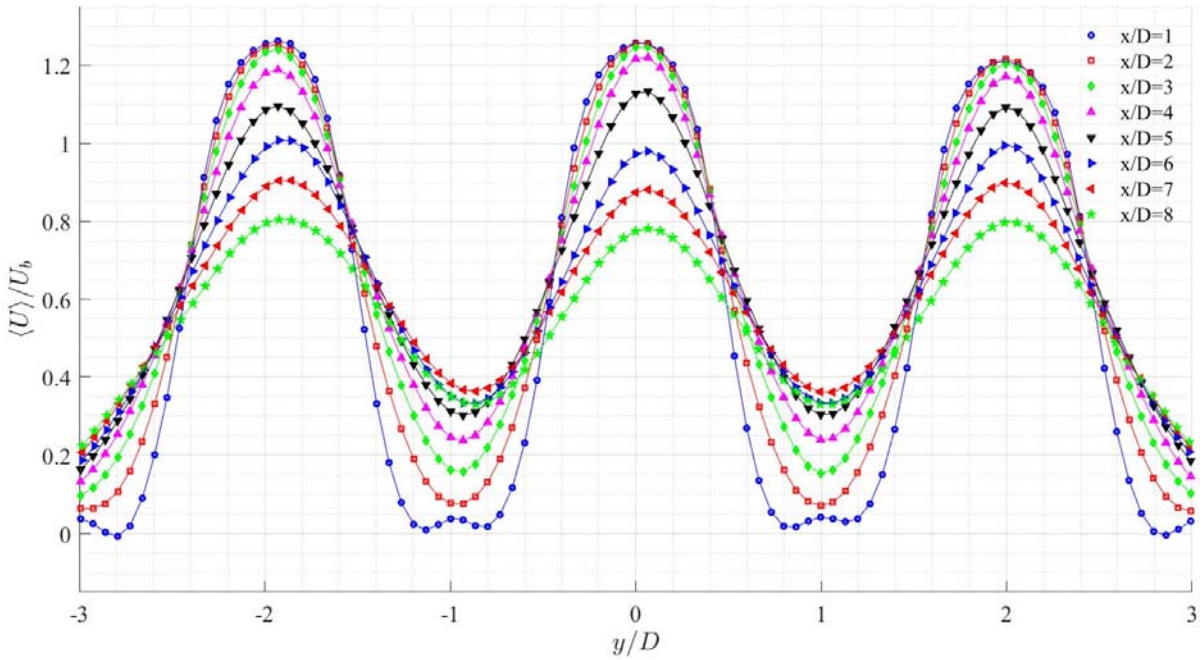

a) Case 1 U_{bulk} = 11.38 m/s

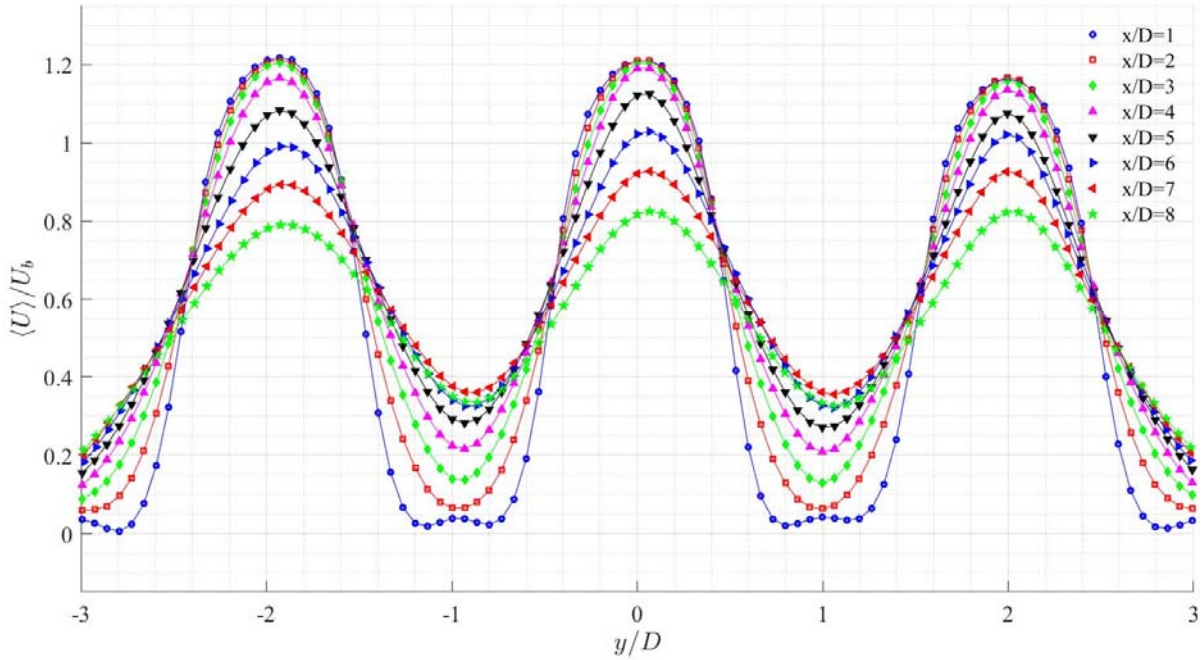

b) Case 2 U_{bulk} = 13.27 m/s

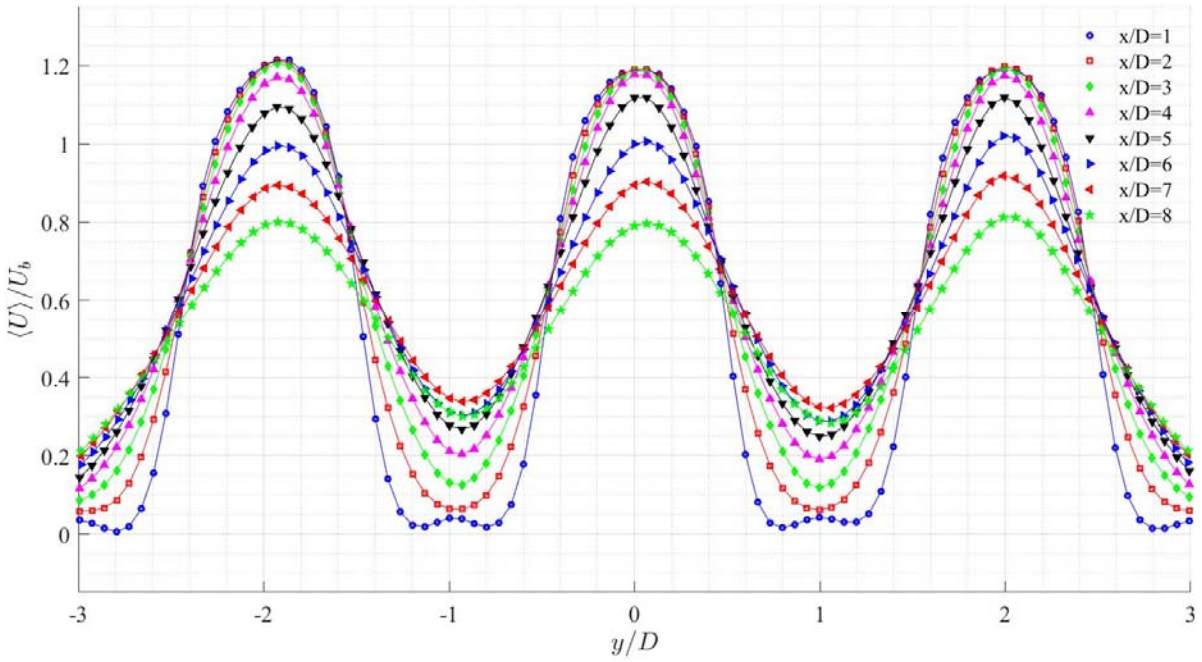

c) Case 3 U_{bulk} = 17.07 m/s

Figure 5: Velocity profile for triple jet

3.3 Reynolds Stresses

Higher order statistics play an important role in dictating the turbulent flow physics. The Reynolds shear stress (uv) for the flow is presented in Figure 6 for both single and triple jets, and is a useful metric to identify shear layers. This Reynolds stress is taken along the center $z = 0$ plane of the jet along various downstream x/D distances. For the single jet cases, the shear stress is mainly positive for $y/D > 0$ and negative for $y/D < 0$, which indicates the presence of a shear layer on either side of the main jet flow. The maximum shear stress is observed at $y/D \approx \pm 0.6$, and is not seen to move too far from that position for the complete data set shown in the figure. This suggests that the position of the shear layer does not drift as the flow progresses in the streamwise direction. It does seem to thicken however evident from the transition of sharper peaks at $x/D = 2$ to the broader distribution at $x/D = 8$. This thickening behavior is indicative of the jet flow spreading as noted from the ensembled-average velocity profiles in Figure 4 and Figure 5. The maximum values for the shear stress also increase with increasing x/D, suggesting higher turbulent fluctuations. But this trend begins to reverse when comparing the $x/D = 7$ and 8 curves, as one would expect when the jet begins to lose its overall momentum. The triple jet shear stress shown in Figure 6 is similar to that of a single jet, but is a superposition of three such profiles. The magnitude of stress is higher for the triple jet since shear exists whenever two regions of different velocities exist in close proximity. There are two such regions for a single jet, one on either side of the bulk jet flow. For the three neighboring jets, these two regions exist for each jet, and therefore provide more opportunity for shear to exist in the domain. Since the jets are not completely isolated from one another, the overall magnitude of the shear is increased (note the scales of Figure 6(a) and (b) differ by an order of magnitude).

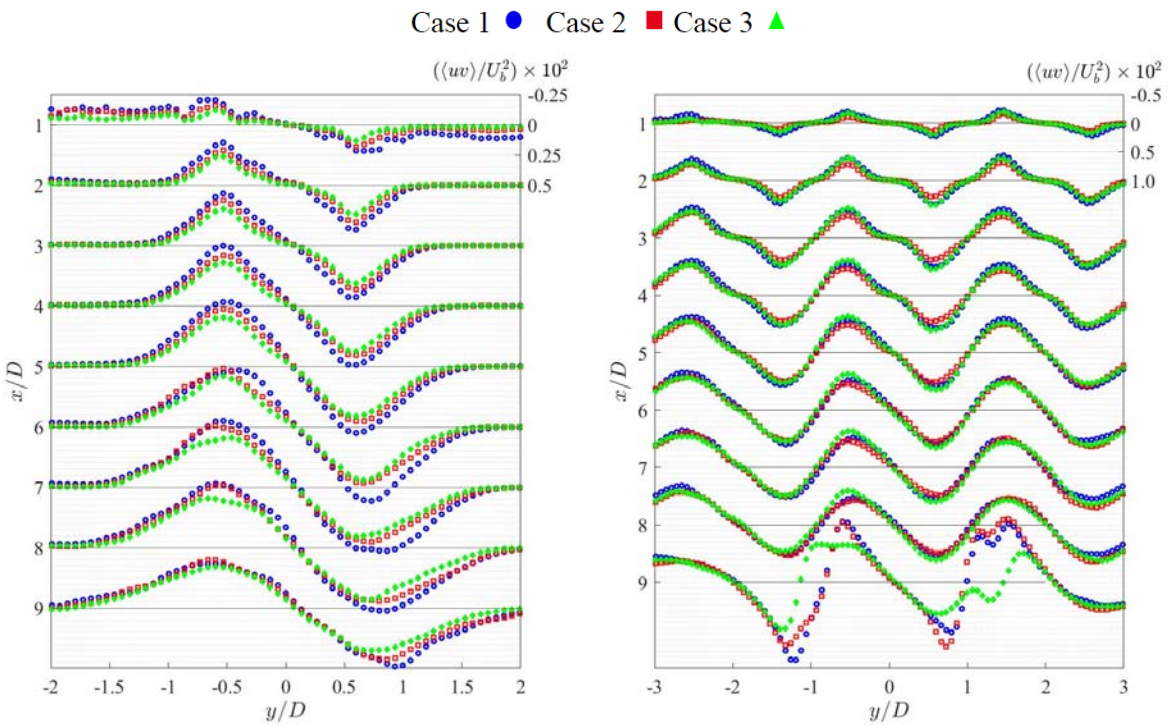

b) Single jet **a) Triple jet**

Figure 6: Reynolds stresses for U_{bulk} = Case 1) 11.38 m/s Case 2) 13.27 m/s Case 3) 17.07 m/s.

3.4 *yz*-Plane Velocity Contours

The ensemble-averaged velocity contours in the yz plane are presented for case 3 for a single and triple jet in Figure 7 and Figure 8, respectively. The rows of these figures represent the velocity contours of the streamwise velocity (u), spanwise velocity (v), or the out of plane velocity (w), while each column is a different downstream location. For the single jet case, the u-velocity contours (top row of Figure 7) are seen to increase in their breadth while the peak velocity decreases, both of which have been noted earlier. However, the x/D = 2 and 3 plots are exceptions to this. It should be noted that for this imaging plane, the velocity in the jet direction is the out of plane component in the PIV measurements. This causes difficulties since the seeder particles resolving that velocity are flowing in the direction of the camera and are more challenging to resolve compared to the two in-plane components. The jet spreading is also evident from the v- and w-velocity contours. (rows 2 and 3, respectively of Figure 7), revealing distinct regions where the velocities direct the flow away from the jet centerline. This is still evident all the way down to x/D = 8. In Figure 8, the triple jet contours are organized in a similar fashion to Figure 7, but in two sections where the first three rows represent x/D = 1, 2, 3 while the last three rows are the x/D = 4, 6, 8 data. Qualitatively, the data is similar to a single jet, especially for the streamwise velocity contours. There are noticeable differences however, when analyzing the v- and w-velocity contours. Although distinct regions are still visible, which take flow away from the jet center, the center jet signature seems to get lost the further downstream one considers. For example, the v-velocity contours at x/D = 8 (5th row and 3rd column of Figure 8) reveal flow away from the outermost region of the three jet collection, but the flow inside of those two bounds no longer has a strong tendency to flow in the y-direction. It does however tend to flow in the z-direction as is evident in the w-velocity contour at the same downstream location (6th row and 3rd column of Figure 8). This stands to reason since the jets are aligned along the y-axis and not the z-axis, and the flow can travel away from the collection of jets more freely in the z-direction.

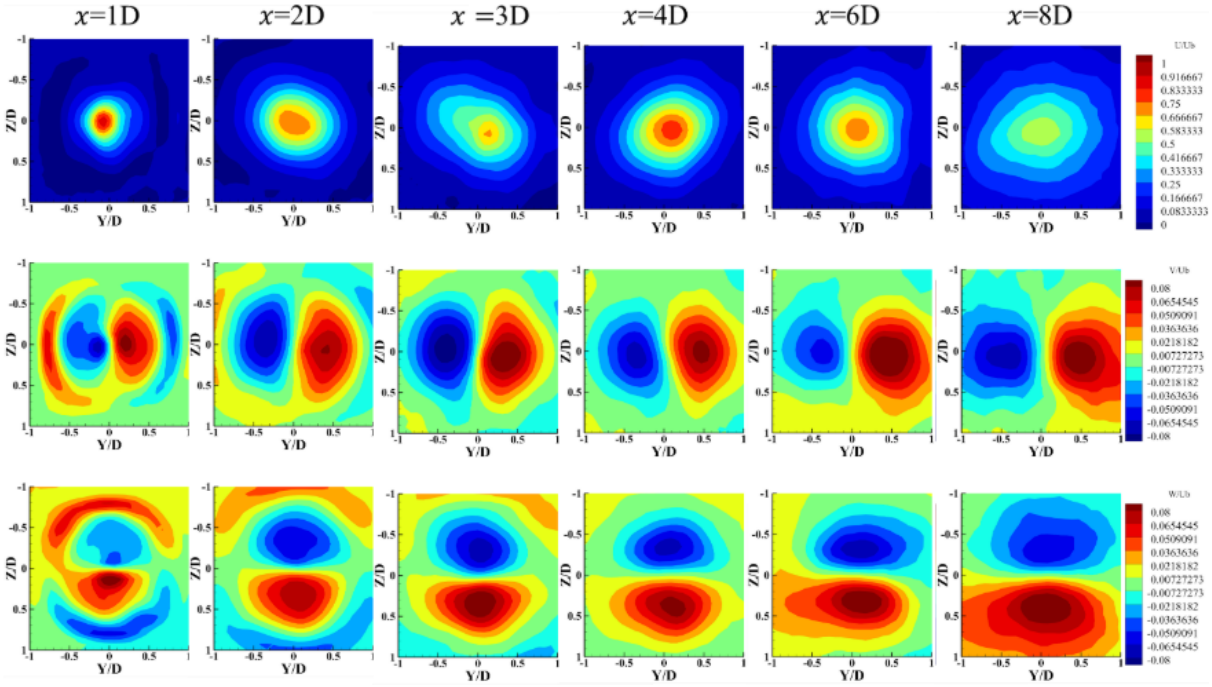

Figure 7: Velocity contours for single jet Case 3 = 17.07 m/s

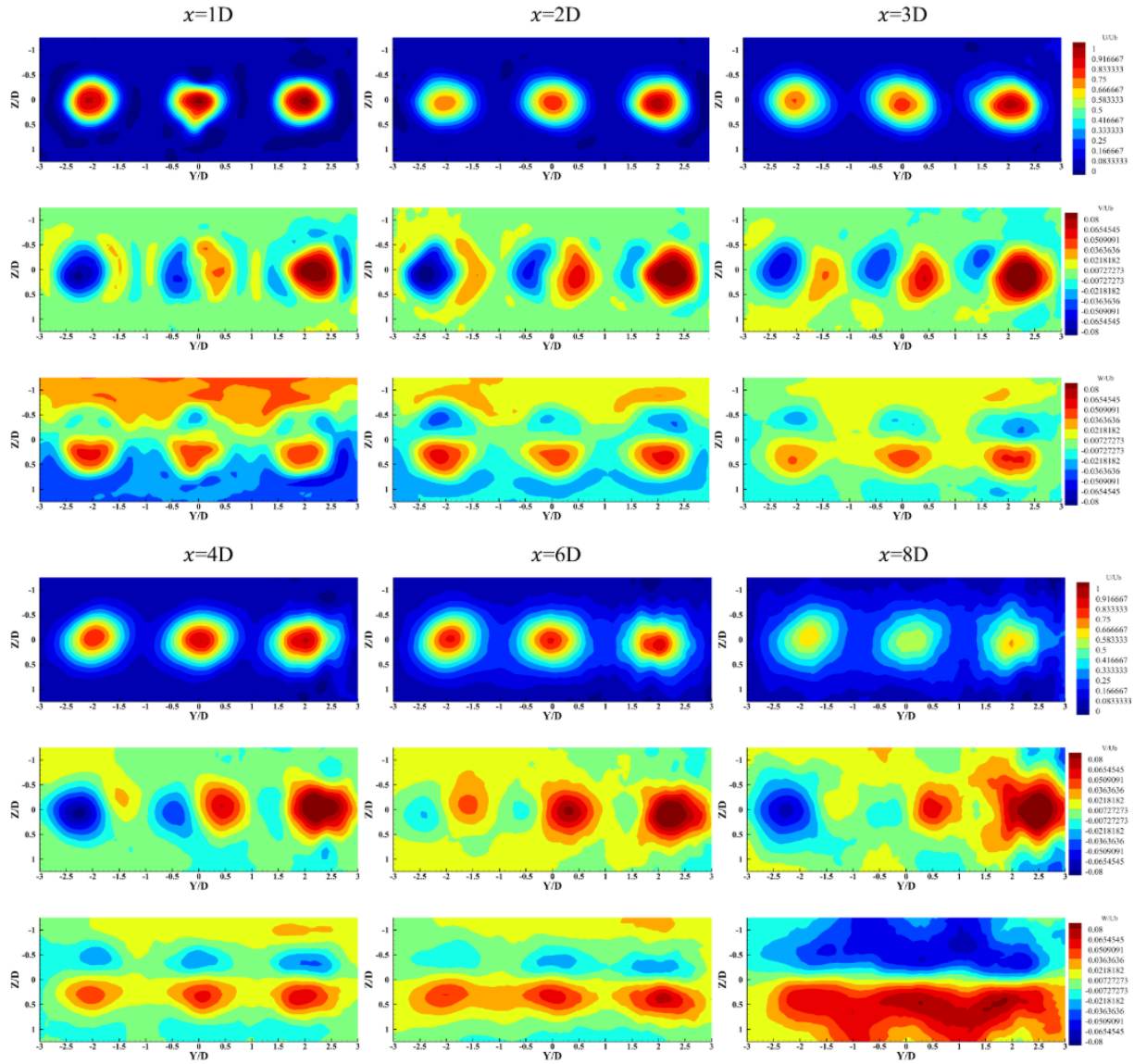

Figure 8: Velocity contour for triple jet Case 3 = 17.07 m/s

4 CONCLUSIONS

The flow interactions between an impinging single jet and a triple jet on a flat plate are considered. The three cases present in this study consists of three unique bulk velocities. Particle image velocimetry (PIV) measurements are taken in two separate but overlapping regions of interest in the downstream direction, and stitched together for each trial and each case. Velocity profiles and velocity contours are measured in both the xy and yz planes. Reynolds shear stresses (uv) are compared at multiple downstream locations for both the single and triple jet. The Reynolds stresses in the triple jet are larger in magnitude than the single jet, suggesting the spacing is such that the presence of neighboring jets is non-negligible. The yz plane contours further reveal the difference in jet spreading between a single and triple jet configuration.

ACKNOWLEDGMENT

This research is being performed using funding received from the DOE Office of Nuclear Energy's Nuclear Energy University Program.

NOMENCLATURE

x	streamwise direction		u	streamwise fluctuating velocity (m/s)
y	spanwise direction		v	spanwise fluctuating velocity (m/s)
z	out of plane direction		w	out of plane fluctuating velocity (m/s)
D	jet diameter	(m)	uv	Reynolds shear stress (m^2/s^2)
U_{bulk}	bulk velocity variable	(m/s)		
$<U>$	ensemble-averaged velocity	(m/s)		

REFERENCES

[1] B. Weigand and S. Spring, "Multiple jet impingement– a review," *Heat Transfer Research,* vol. 42, 2011.

[2] R. S. Snedeker, "A study of free jet impingement. Part 1. Mean properties of free and impinging jets," *Journal of fluid Mechanics,* vol. 45, pp. 281-319, 1971.

[3] D. Reungoat, N. Rivière, and J.-P. Fauré, "3C PIV and PLIF measurement in turbulent mixing round jet impingement," *Journal of Visualization,* vol. 10, pp. 99-110, 2007.

[4] M. Fairweather and G. Hargrave, "Experimental investigation of an axisymmetric, impinging turbulent jet. 1. Velocity field," *Experiments in Fluids,* vol. 33, pp. 464-471, 2002.

[5] P. E. Dimotakis, "Turbulent mixing," *Annu. Rev. Fluid Mech.,* vol. 37, pp. 329-356, 2005.

[6] C. E. Clifford, A. D. Fradeneck, A. M. Oler, S. Salkhordeh, and M. L. Kimber, "Computational study of full-scale VHTR lower plenum for turbulent mixing assessment," *Annals of Nuclear Energy,* vol. 134, pp. 101-113, 2019.

[7] S. Salkhordeh, C. Clifford, A. Jana, and M. L. Kimber, "Large Eddy Simulations of scaled HTGR lower plenum for assessment of turbulent mixing," *Nuclear Engineering and Design,* vol. 334, pp. 24-41, 2018.

[8] I. Craig, C. Hoff, P. Kristo, and M. Kimber, "A validation experiment for turbulent mixing in a collated jet," in *Proceedings of the ASME/JSME/KSME 2019 Joint Fluids Engineering* San Francisco, CA, USA, 2019, pp. AJKFluids2019-4981.

[9] C. Oh, E. Kim, R. Schultz, M. Patterson, and D. Petti, "Thermal hydraulics of the very high temperature gas cooled reactor," Idaho National Laboratory (INL)2009.

[10] H. M. McIlroy, D. M. McEligot, and R. J. Pink, "Measurement of flow phenomena in a lower plenum model of a prismatic gas-cooled reactor," *Journal of Engineering for Gas Turbines and Power,* vol. 132, p. 022901, 2010.

[11] D. T. Landfried, P. Kristo, C. E. Clifford, and M. Kimber, "Design of an experimental facility with a unit cell test section for studies of the lower plenum in prismatic high temperature gas reactors," *Annals of Nuclear Energy,* vol. 133, pp. 236-247, 2019.